

THE FREEZING OF SMALL TYNDALL FIGURES IN ICE

By SHINJI MAE

(Water Research Institute, Nagoya University, Nagoya, Japan)

ABSTRACT. Tyndall figures, small thin discs of liquid water containing a vapour cavity, were formed in the centres of grains of pure, polycrystalline ice and observed while freezing and growing. The freezing experiments showed that the rate of decrease in the radius of a Tyndall figure does not depend upon the radius of the figure, but does depend upon the thickness, h . Below a transition thickness, $h_t = 12 \mu\text{m}$, the rate of decrease of the radius varied with h^{-2} ; above h_t , with h^{-1} . For growing figures the transition thickness was $h_{tg} \approx 10 \mu\text{m}$, and was defined in such a way that when $h > h_{tg}$ perturbations with wavelengths greater than $10^2 \mu\text{m}$ formed on the side faces of the Tyndall figures.

RÉSUMÉ. *Le refroidissement de petites figures de Tyndall dans la glace.* Des figures de Tyndall, minces petits disques d'eau liquide contenant une cavité remplie de vapeur, ont été formées au centre de grains de glace polycristalline pure et observées au cours de leur refroidissement et de leur croissance. Les expériences de refroidissement ont montré que la vitesse de changement dans le rayon des figures de Tyndall ne dépend pas de leur rayon mais dépend de leur épaisseur h . En dessous d'une épaisseur de transition $h_t = 12 \mu\text{m}$, la vitesse de variation du rayon varie comme h^{-2} ; au dessus de h_t , comme h^{-1} . Une même épaisseur de transition à la croissance, $h_{tg} \approx 10 \mu\text{m}$, a été observée dans les figures en cours de croissance et a été définie de manière à ce que lorsque $h > h_{tg}$ des perturbations avec des longueurs d'onde supérieures à $10^2 \mu\text{m}$ se forment sur la face latérale des figures de Tyndall.

ZUSAMMENFASSUNG. *Das Gefrieren kleiner Tyndall-Figuren in Eis.* Tyndall-Figuren, kleine, dünne Scheiben flüssigen Wassers mit Dampfhohlräumen, bildeten sich in den Zentren der Körner klaren, polykristallinen Eises; sie wurden während des Gefrierens und Wachsens beobachtet. Die Gefrierversuche zeigten, dass die Geschwindigkeit, mit der der Radius der Tyndall-Figuren sich ändert, nicht vom Radius der Figuren, wohl aber von ihrer Dicke h abhängt. Unterhalb einer Übergangsdicke $h_t = 12 \mu\text{m}$ ist die Änderungsgeschwindigkeit des Radius proportional zu h^{-2} , oberhalb von h_t jedoch proportional zu h^{-1} . Auch beim Wachsen der Figuren wurde eine Übergangsdicke $h_{tg} \approx 10 \mu\text{m}$ festgestellt, die sich folgendermassen definieren lässt: Solange $h > h_{tg}$ ist, bilden sich Störungen mit Wellenlängen grösser als $10^2 \mu\text{m}$ an den Seitenflächen der Tyndall-Figuren.

1. INTRODUCTION

Tyndall figures are produced from the internal melting of ice. Nakaya (1956) investigated a variety of different Tyndall figures in ice single crystals. He showed that because of the density difference between ice and water, they consisted of a water phase and a vapour cavity. His work clearly showed the importance of understanding these figures as a step in the understanding of the growth of ice from supercooled water.

One of the most intractable problems in studying the crystal growth of ice or determining the ice-water interfacial energies is the difficulty of avoiding the effects of impurities. Using Tyndall figures eliminates most of the problem.

Although, as Nakaya has shown, it is possible to grow many kinds of Tyndall figures, the experiments described herein are limited to the freezing and growth of small discs in polycrystalline ice as illustrated in Figure 1. Cross-sections such as are shown in Figure 2, indicate that two planar faces are parallel and perpendicular to the c -axis whilst the side faces are slightly curved. The black centres are vapour cavities which have the same thickness as the water phase. The radii, r of the Tyndall figure, and r_v of the vapour cavity, always exceed the thickness, h ; the smallest value for r_v/h being nearly 2.

2. EXPERIMENTAL PROCEDURE

Cylinders of ice in which the average grain size was approximately 5 mm were grown from degassed, distilled, de-ionized water (the total molar fraction of the impurities $\ll 10^{-7}$) in stainless-steel containers 130 mm in diameter and 150 mm long. The individual specimens were cut from these cylinders into discs approximately 40 mm in diameter and 20 mm thick.

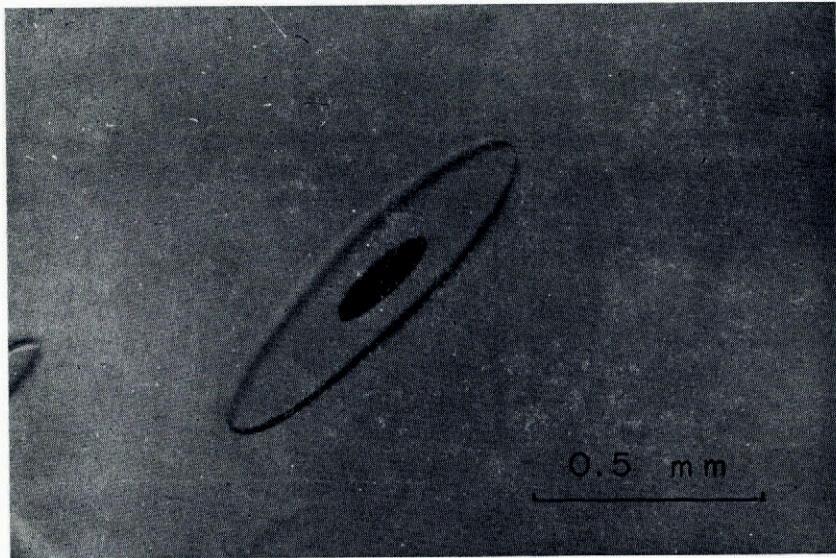


Fig. 1. Small Tyndall figure in ice with vapour cavity.

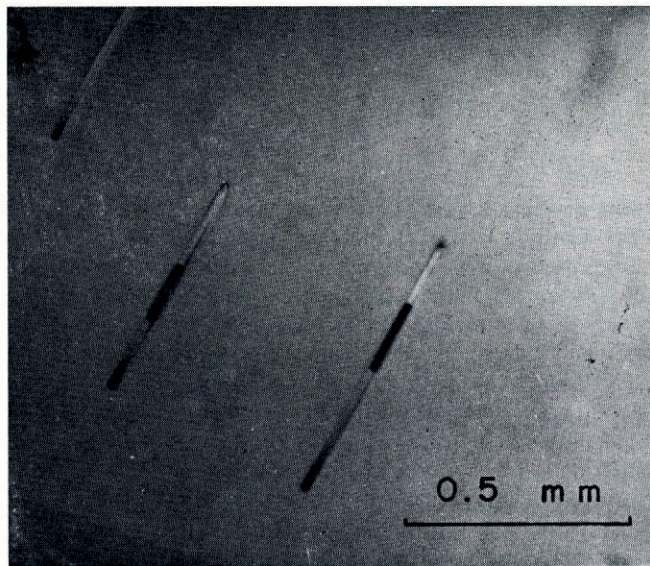


Fig. 2. Cross-sections of Tyndall figures in ice.

Tyndall figures were produced by focusing light from a small lamp into an area $2\text{ mm} \times 2\text{ mm}$ after the specimens reached the melting point as indicated by veins of water forming along the intersections of three grain boundaries (Nye and Mae, 1972) and the melting of the grain boundaries. The thickness of the water film in the boundaries was about $10\text{ }\mu\text{m}$ and the decrease of the melting point due to impurities might be 10^{-5} deg. The solubility of impurities in ice is very low. Therefore, the impurity effect to the freezing of

Tyndall figures may be neglected. In the freezing experiment only one Tyndall figure was formed in the centre of one grain, although Figure 2 shows a few figures in a grain. As freezing began following radiation, the radius and the thickness of the figures was measured microscopically and photographically (see Figs 3, 4, 5).

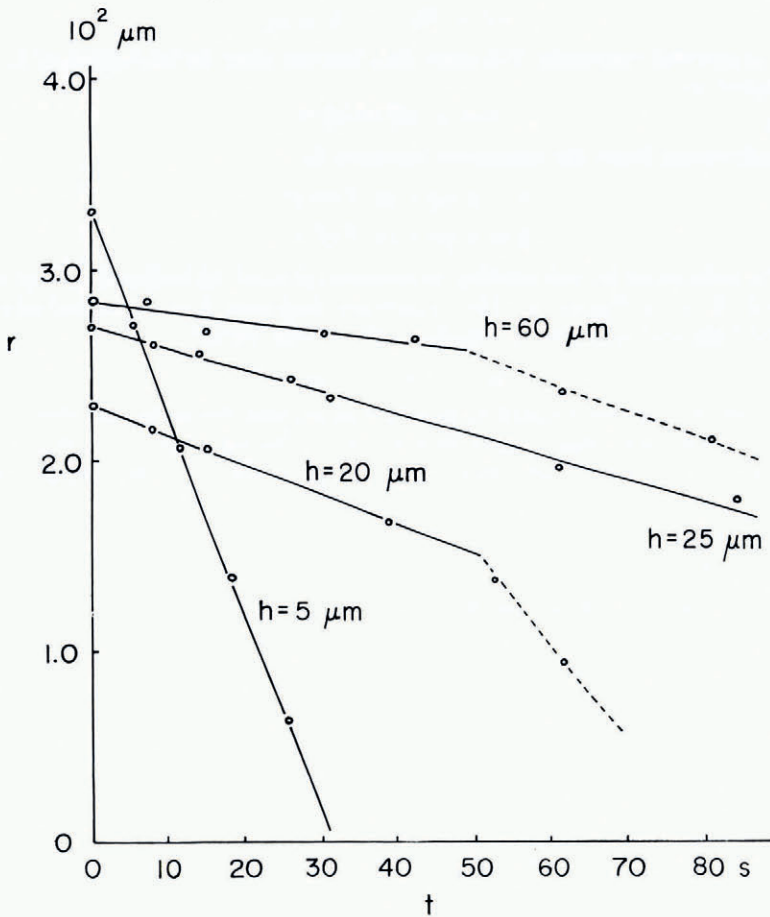


Fig. 3. Relation between the radius r and time t in freezing Tyndall figures. Stages are indicated by solid and dashed lines.

3. EXPERIMENTAL RESULTS

Figure 3 and 4 illustrate the relation of the radius r and the thickness h to time t . In these figures $t = 0$ when the measurements begin, not when the freezing begins. As may be seen in the figures, the curves have two stages; the first marked by a solid line and the second by a dashed line. In the first stage r decreases proportionately with t as h remains constant within the experimental error. In the second stage, $-\dot{r}$, the rate of the decrease of r , increases, and h decreases with t . The transition from the first to the second stage occurs when r_v/h approaches $\frac{3}{2}$. In this stage the vapour cavity of the figure becomes ellipsoidal. Because of the complexity of the figures in this second stage, this paper concerns itself with the first stage only.

Figure 5 illustrates the relation between $-\dot{r}$, the rate of decrease of r with t , and h . Here two regimes are separated by the transitional thickness h_t . In the first regime, I, $-\dot{r}$ is asymptotically proportional to h^{-2} as h decreases:

$$-\dot{r} = \alpha h^{-2} \quad h \ll h_t \quad (1)$$

where α is a numerical constant. In the second regime, II, $-\dot{r}$ is asymptotically proportional to h^{-1} :

$$-\dot{r} = \beta h^{-1} \quad h \gg h_t \quad (2)$$

where β is a numerical constant. We may thus assume that for all values of h , the relation may be expressed as:

$$-\dot{r} = \alpha h^{-2} + \beta h^{-1}. \quad (3)$$

α and β are calculated from the measured values to be:

$$\alpha = 2.95 \times 10^{-16} \text{ m}^3 \text{ s}^{-1}, \quad (4)$$

$$\beta = 1.90 \times 10^{-11} \text{ m}^2 \text{ s}^{-1}. \quad (5)$$

The ratio $-\dot{r}$ is calculated by substituting Equations (4) and (5) in Equation (3) and is shown by the thinner curve in Figure 5. The transition thickness h_t is quantitatively defined by setting the first term in Equation (3) equal to the second term:

$$h_t = \alpha/\beta = 12 \text{ } \mu\text{m}.$$

During the growth of the Tyndall figures, a transitional thickness was observed, $h_{tg} \approx 10 \text{ } \mu\text{m}$. When h was less than this transitional thickness, the figures were in the form of a thin disc and when h exceeded it they became truncated cones with the perturbed side faces.

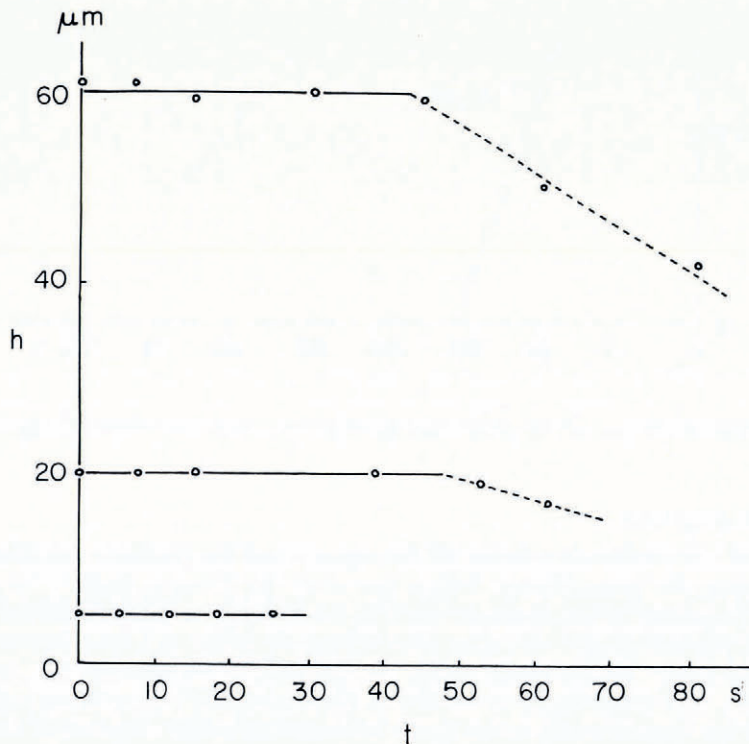


Fig. 4. Relation between thickness h and time t in freezing Tyndall figures. Stages are indicated by solid and dashed lines.

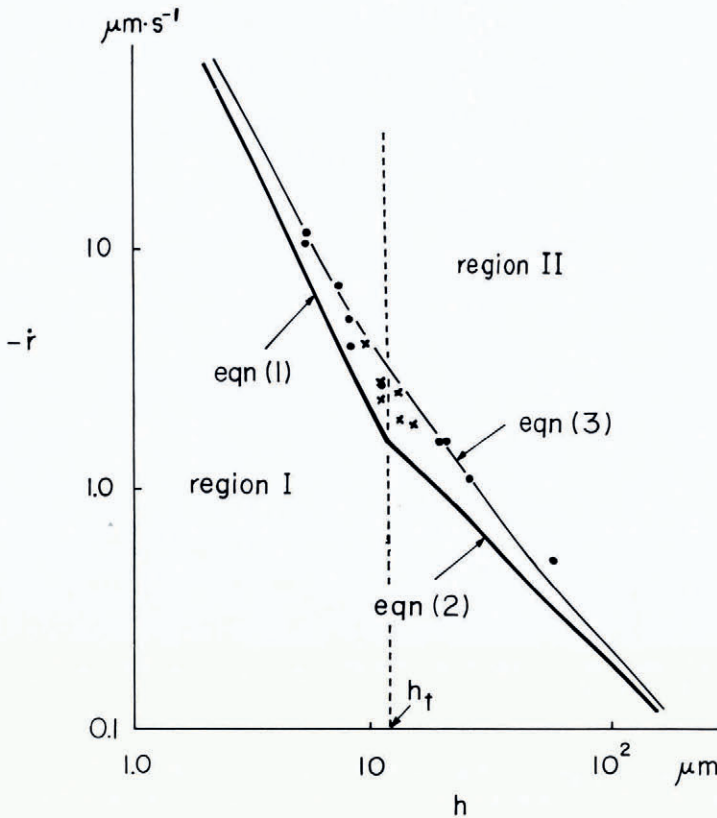


Fig. 5. The rate of decrease of the radius $-\dot{r}$ in freezing Tyndall figures is plotted as a function of the thickness, h . ● indicates measurements made from photographs and x measurements made with the microscope.

These features are illustrated in Figure 6 in which $h < h_{\dagger g}$ is denoted by a dashed arrow and $h > h_{\dagger g}$ by a solid one. A detailed description of the morphology of growing Tyndall figures will be given in a subsequent paper.

4. DISCUSSION

In Figures 3 and 4 it is shown that the growth rate parallel to c -axis is negligible compared with that perpendicular to c -axis. Such anisotropy in the growth kinetics was observed by Hillig (1958). Therefore, the anisotropy of the freezing of disc-shaped Tyndall figures is the result of a strong anisotropy in interfacial growth kinetics and not of anisotropic heat flow.

We assume that the relation between \dot{r} and h is expressed by Equation (3). However, this relationship is approximate and not exact because the observed range of h is not sufficiently wide and our observation is mainly concentrated in a range of superposition of Equations (1) and (2).

Arakawa (1955) carried out a very interesting observation on the growth of disc-shaped ice crystals on supercooled water and his observation is very important in the study of the morphological stability of disc-shaped crystals. Tyndall figures are considered to be negative disc-shaped crystals of ice and we can apply theories on the growth of crystals to the melting of Tyndall figures. In the case of the growth of ice discs floating on supercooled water we

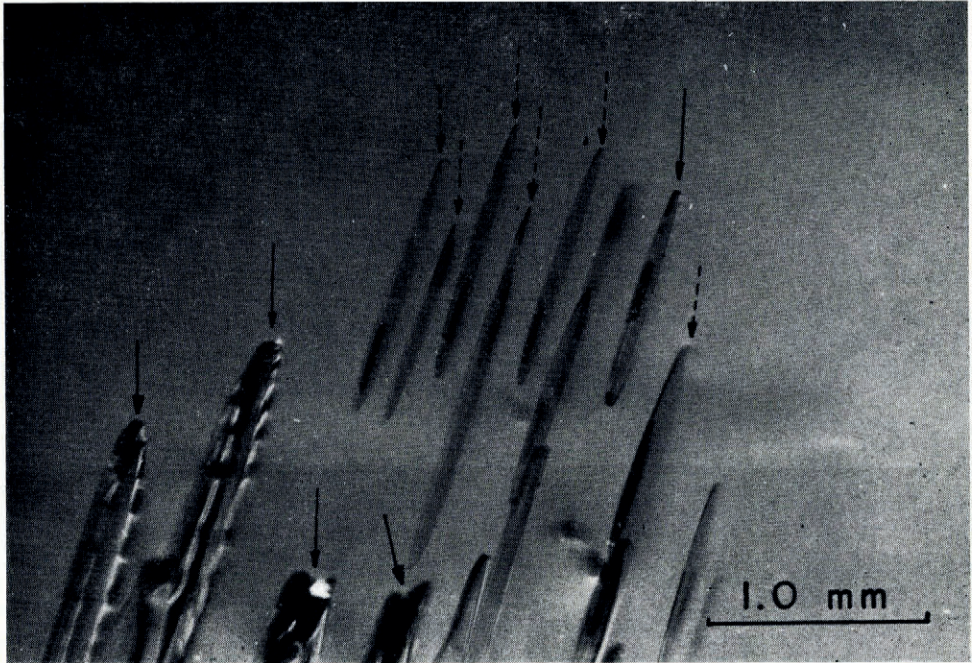


Fig. 6. Growing Tyndall figures in ice. Solid arrows indicate Tyndall figures with perturbed surfaces and dashed arrows indicate figures with smooth surfaces.

have to take into account convection in air and water, but in the melting experiment motion of vapour cavities in Tyndall figures was not observed and it is unnecessary to consider such convection. Therefore, the melting of Tyndall figures is a suitable case for comparison of experimental results with theoretical models for the growth of disc-shaped crystals.

In the growth of Tyndall figures it was found that there was a transitional thickness, $10\ \mu\text{m}$, above which disc-shaped Tyndall figures became unstable in their morphology. This shows that it is important to take thickness into account in consideration of the morphological stability of disc-shaped crystals. Although it is interesting that $h_t \approx h_{tg}$ as described in section 3, the reason why these two values are equal is not clear. If we could obtain an exact solution of the freezing rate of Tyndall figures, the reason should be explained.

MS. received 5 October 1973 and in final form 27 June 1975

REFERENCES

- Arakawa, K. 1955. The growth of ice crystals in water. *Journal of Glaciology*, Vol. 2, No. 17, p. 463–67.
- Hillig, W. B. 1958. The kinetics of freezing of ice in the direction perpendicular to the basal plane. (In Doremus, R. H., and others, ed. *Growth and perfection of crystals. Proceedings of an international conference on crystal growth, held at Cooperstown, New York, Aug. 27–29, 1958*. Edited by R. H. Doremus, B. W. Roberts, D. Turnbull. New York, John Wiley and Sons Inc. p. 350–60.)
- Nakaya, U. 1956. Properties of single crystals of ice, revealed by internal melting. *U.S. Snow, Ice and Permafrost Research Establishment. Research Report 13*.
- Nye, J. F., and Mae, S. 1972. The effect of non-hydrostatic stress on intergranular water veins and lenses in ice. *Journal of Glaciology*, Vol. 11, No. 61, p. 81–101.